

# Arbitrary structured quantum emission with a multifunctional imaging metalens

Chi Li<sup>1#\*</sup>, Jaehyuck Jang<sup>2#</sup>, Trevon Badloe<sup>3#</sup>, Tieshan Yang<sup>1,8</sup>, Joohoon Kim<sup>3</sup>, Jaekyung Kim<sup>3</sup>, Minh Nguyen<sup>1</sup>, Stefan A. Maier<sup>4,5</sup>, Junsuk Rho<sup>2,3,6,7\*</sup>, Haoran Ren<sup>4\*</sup>, Igor Aharonovich<sup>1,8</sup>

1. School of Mathematical and Physical Sciences, University of Technology Sydney, Ultimo, New South Wales 2007, Australia
2. Department of Chemical Engineering, Pohang University of Science and Technology (POSTECH), Pohang 37673, Republic of Korea
3. Department of Mechanical Engineering, Pohang University of Science and Technology (POSTECH), Pohang 37673, Republic of Korea
4. School of Physics and Astronomy, Monash University, Melbourne, Victoria, Australia
5. Department of Physics, Imperial College London, London SW7 2AZ, United Kingdom
6. POSCO-POSTECH-RIST Convergence Research Centre for Flat Optics and Metaphotonics, Pohang 37673, Republic of Korea
7. National Institute of Nanomaterials Technology (NINT), Pohang 37673, Republic of Korea
8. ARC Centre of Excellence for Transformative Meta-Optical Systems, University of Technology Sydney, Ultimo, New South Wales 2007, Australia

# These authors contributed equally to this work

Email address: [chi.li@uts.edu.au](mailto:chi.li@uts.edu.au); [jsrho@postech.ac.kr](mailto:jsrho@postech.ac.kr); [haoran.ren@monash.edu](mailto:haoran.ren@monash.edu)

## Abstract

*Structuring light emission from single-photon emitters in multiple degrees of freedom is of a great importance for quantum information processing towards higher dimensions. However, traditional control of emission from quantum light sources relies on the use of multiple bulky optical elements or nanostructured resonators with limited functionalities, constraining the potential of multi-dimensional tailoring. Here we introduce the use of an ultrathin polarisation-beam-splitting metalens for the arbitrary structuring of quantum emission at room temperature. Owing to the complete and independent polarisation and phase control at a single meta-atom level, the designed metalens enables simultaneous imaging of quantum emission from ultra-bright defects in hexagonal boron nitride and imprinting of an arbitrary wavefront onto orthogonal polarisation states of the sources. The hybrid quantum metalens enables simultaneous manipulation of multiple degrees of freedom of a quantum light source, including directionality, polarisation, and orbital angular momentum. The demonstrated arbitrary wavefront shaping of quantum emission in multiple degrees of freedom could unleash the full potential of solid-state SPEs for their use as high-dimensional quantum sources for advanced quantum photonic applications.*

## Main

Quantum emission is pivotal to the realisation of photonic quantum technologies, cryptography, communications, sensing, and computing<sup>1,2</sup>. Solid-state single photon emitters (SPEs) such as defects in hexagonal boron nitride (hBN) operate at room temperature and are highly desired due to their robustness and brightness<sup>3,4,5</sup>. The conventional way to collect photons from SPEs often relies on a high numerical aperture (NA) objective lens or employment of microstructured antennas such as nanopillars<sup>6</sup>. While the efficiency of photon collection can be high, these tools lack the capability to manipulate quantum emission - particularly in regard to directionality or phase. Consequently, for achieving any desired structuring of the emitted quantum light source, multiple bulky optical elements such as polarisers and phase plates are inevitably required.

The ability to arbitrarily structure light in its multi-dimensions is of great importance for quantum light sources<sup>7,8,9,10,11,12,13</sup>. In this respect, metasurfaces have transformed the landscape of photonic design, propelling major technological advances spanning from optical imaging<sup>14,15</sup>, displays<sup>16</sup>, and holography<sup>17,18,19</sup>, to Lidar<sup>20</sup> and molecular sensing<sup>21</sup>. Recently, the direct integration of nanoscale emitters into nanostructured resonators and metasurfaces have been realised to collect the SPEs emission<sup>22,23</sup> and demonstrate basic tailoring of the emission<sup>24,25,26</sup>. These initial works constituted the necessity to design and engineer a multifunctional metalens, capable of multi-dimensional structuring of quantum emission.

Here we address this vision, by designing and engineering a multifunctional imaging metalens, capable of tailoring the directionality, polarisation, and orbital angular momentum (OAM) degrees of freedom simultaneously (Fig. 1a). Specifically, we utilise the metalens to demonstrate a multidimensional structuring of quantum emission from SPEs in hBN, operating at room temperature. Since our designed meta-atoms in the metalens can achieve complete and independent polarisation and phase manipulation, it is possible to encode different wavefronts onto orthogonal polarisations of SPEs. Hence, we demonstrate an arbitrary shaping of the directionality of quantum emission by adding distinctive phase gratings selective to orthogonal polarisations onto the metalens profile, which are represented by different spots in momentum space of the metalens (Fig. 1b). In addition, we show that different helical wavefronts can be further added onto the metalens profile, leading to the generation of distinctive OAM modes in orthogonal polarisations of SPEs, which are represented by doughnut-shaped spots with different sizes in momentum space (Fig. 1c). The demonstrated arbitrary wavefront shaping of quantum emission in multiple degrees of freedom could unleash the full potential of solid-state SPEs to be used as high-dimensional quantum sources for advanced quantum photonic applications.

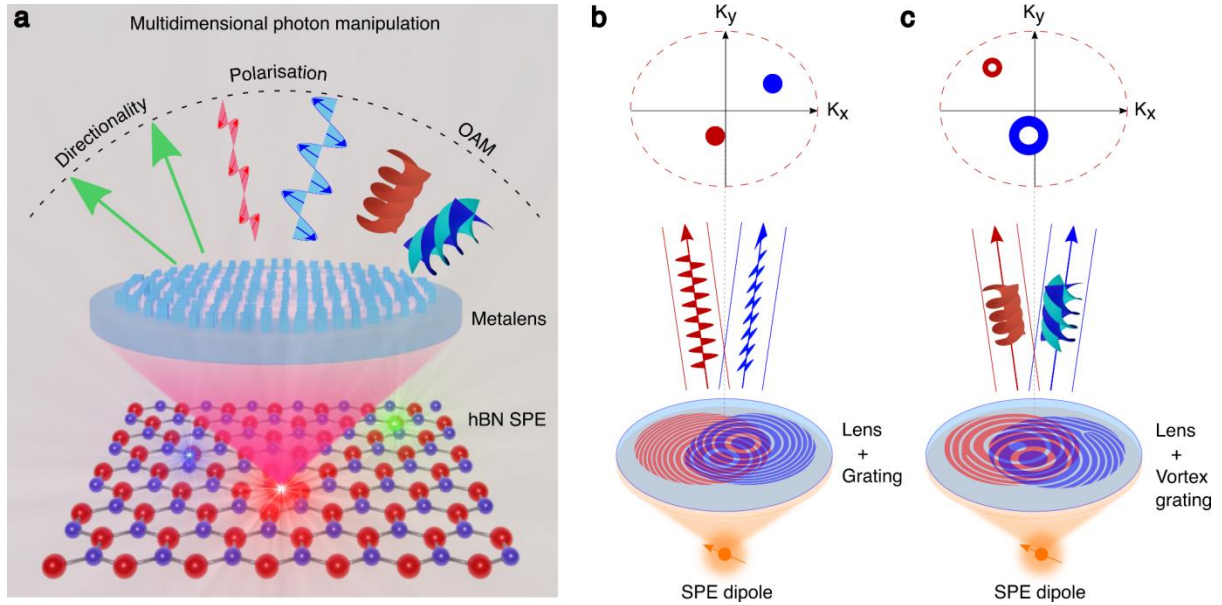


**Fig. 1: Schematics of multidimensional manipulation of hBN quantum emission using a multifunctional metalens.** *a.* Directional photon splitting, polarisation control and subsequent orbital angular momentum encoding. The green arrows stand for the directionality control of SPE emission collected by the metalens. Two sine waves indicate the split of SPE emission into two orthogonal polarised streams. The two helical beams indicate a further dressing by OAM. *b, c.* Enlarged views of each encoding concept where grating and vortex grating are adapted to structure the photons in extra dimensions. In addition, the directionality of orthogonal linear polarisations is well inherited and projected as the red and blue spots in the momentum ( $k$ ) space.

## Results and discussion

We design a polarisation sensitive metalens to decompose the emission from hBN into two orthogonal linear polarisation (LP) states along the  $x$ - and  $y$ -axis directions, denoted as LP $_x$  and LP $_y$ , respectively. We chose the LP to match the linearly polarised emission profile of SPEs in hBN. However, we note that the design could be adapted for other orthogonal polarizations of light, such as left and right circularly polarised light. Taking advantage of the multiplexing possibility offered by the metalens, we add multiple functionalities - specifically structuring the OAM of quantum emission. To achieve this, we design cuboid shaped meta-atoms with a fixed height ( $H$ ) and varying length ( $l$ ), and width ( $w$ ), arranged in a square lattice with periodicity ( $P$ ), as shown in Fig. 2a. We choose low-loss hydrogenated amorphous silicon (a-Si:H)<sup>27,28</sup> as the material of the metalens due to its negligible extinction coefficient in the visible emission of hBN SPEs (Fig. S1). We assume that the meta-atoms act as truncated rectangular waveguides, so with a sufficiently large  $H$ , the required independent phase modulation ( $\varphi$ ) to the incident LP $_x$  and LP $_y$  light from  $0$ - $2\pi$  can be achieved by varying the transverse dimensions of  $l$  and  $d$ . Subsequently, we perform a parameter sweep of different values for  $H$ ,  $l$ , and  $d$ , to design a meta-atom for each of the required  $\varphi$  for LP $_x$  and LP $_y$  using an in-house-built rigorous coupled wave analysis (RCWA) solver. Eight phase steps between  $0$ - $2\pi$  are successfully achieved from various values of  $l$  and  $d$  at a fixed  $H$  of 550 nm (Fig. 2b). Any meta-atoms with a transmission lower than 80% were rejected, and the meta-atoms with the closest  $\varphi$  for both LP $_x$  and LP $_y$  were determined for each required phase step. The chosen  $8 \times 8$  meta-atoms show an average transmission of 94%, and average discrepancy in  $\varphi$  of  $\sim 0.09$  rad. The phase maps of the metalens with a numerical aperture (NA) of 0.869 were designed to collect and collimate the emission from SPEs. To realise the control of directionality of LP $_x$  and LP $_y$  emissions, two independent linear phase gratings can be further implemented onto the lens profile of the orthogonal polarisations. The angle of the deflection depends on the grating period that the phase gradient cycles over  $2\pi$ . As an example, the required phase maps for LP $_x$  and LP $_y$  to deflect beams in the  $\pm x$  direction are shown in Fig. 2c.

To realise the designed metalens, we employ standard electron beam lithography followed by a dry etching process (see Methods). Optical microscope as well as scanning electron microscope images are shown in Fig. 2d. The cuboid shaped meta-atoms are fabricated with high accuracy across the metalens, albeit with a slightly slanted sidewall. We experimentally characterise the metalens performance through its point spread function (PSF) by illuminating the sample with collimated light (Fig. 2e). As a result, the metalens efficiently focuses and deflects the orthogonal polarisation components into two diffraction-limited focal spots shifted along a horizontal line. A small portion of light is focused at the focal point corresponding to the opposite polarisation. This could be attributed to imperfect linear polarisation of incident light due to optical components such as the polariser and the half wave plate. As a result, our experimental characterisation has verified the design of a polarisation beam-splitting metalens. Switching the illumination source to a dipole-like incidence, our metalens with a high NA can efficiently collect large angle incidence, collimate, and deflect orthogonal polarisations of LP<sub>x</sub> and LP<sub>y</sub> into different directions, with two distinct collimated beams propagate at around 16° (Fig. 2f). The dipole collection efficiency for the incident LP<sub>x</sub> and LP<sub>y</sub> polarised light is 16.4% and 17.1%, respectively, and the corresponding power signal-to-noise ratio (SNR) is around 11.3 and 14.9 dB (Supplementary Table 1).

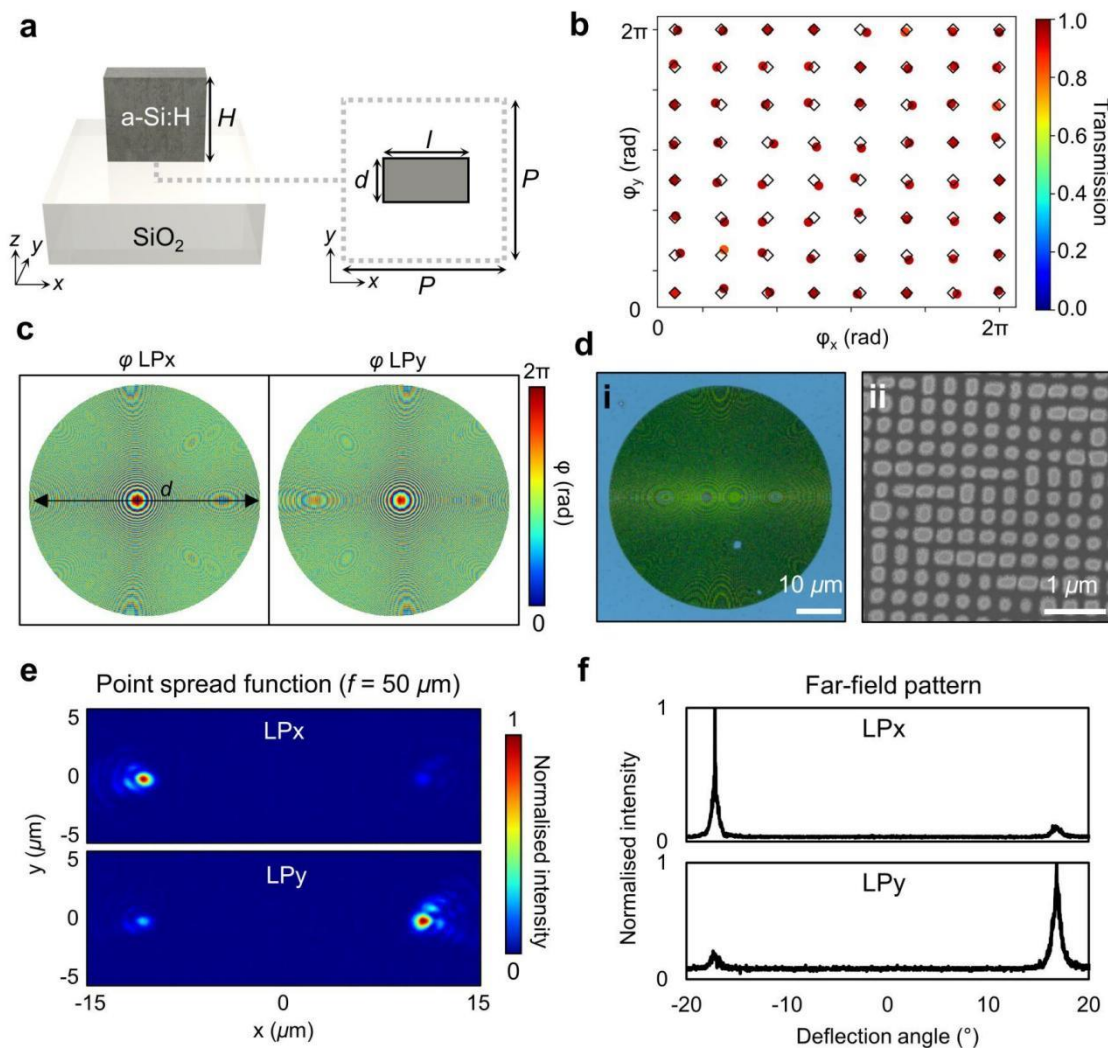


**Fig. 2: Design and characterisation of a polarisation beam-splitting metalens.** *a*, Schematic of the meta-atom blocks from amorphous silicon on silicon oxide. *b*, Calculated phase delay and transmission library of meta-atoms covering  $2\pi$  for both LP<sub>x</sub> and LP<sub>y</sub> light. The average transmission is 94%. *c*,

*Implemented phase maps for the metalens and gradient functions for LPx and Lpy incidence. d, Images of the fabricated metalens taken with an (i) optical microscope and (ii) scanning electron microscope. e, Measured point spread function of the metalens for LPx and Lpy plane-wave incidence f, 1D profile of the measured far-field pattern of the metalens under LPx and Lpy dipole-like illumination.*

To prepare the hBN SPEs, the hBN solution containing SPEs is prepared on a glass substrate (see Methods). We choose a SPE with emission at  $\sim 610$  nm, to match the designed metalens. First, the emitters are characterised using a conventional confocal microscope with a Hanbury Brown-Twiss interferometer to confirm the quantum nature of emitted light, as shown in fig. 3a. Briefly, the hBN emitters are excited using a green (532 nm) laser and the emission is collected using same objective. The chosen SPE is shown in Fig. 3b, with a dominant zero-phonon line (ZPL) centred at 591 nm and a minor phonon sideband (PSB). Photon anti-bunching behaviour is confirmed by recording the second-order correlation function,  $g^{(2)}(\tau)$ , with a background corrected  $g^{(2)}(0) = 0.05$ . Finally, the SPE dipole orientation is confirmed to be  $106^\circ$  (black arrow) with respect to the laboratory frame, as confirmed by rotating a linear polarizer in the collection path (Fig. 3c).

We now utilise the metalens for multidimensional structuring of the quantum emission of the precharacterised hBN SPE. First, the metalens was used as a collection lens in the transmission path and the LPx direction is set to horizontal ( $90^\circ$ ) as shown in Fig. 3c (red arrow). An SPE dipole-to-metalens LPx intersection angle of  $16^\circ$  is hence derived. As expected, the SPE emission passes through the polarisation beam-splitting metalens and splits into LPx (red curve) and LPy (blue curve) as shown in Fig. 3d. Both photon streams result in sharp spectra with peaks centred at 591 nm, corresponding to the ZPL of the SPE. LPx and LPy polarisation are confirmed with a polarizer and have been used to calibrate the metalens mounting angle. Note, the peak area ratio is  $A_{LPy}/A_{LPx} = 0.19$  which is slightly lower than the anticipated dipole projection ratio  $\tan(16^\circ) = 0.29$  in the orthogonal directions. One possible explanation is the variation of free space to fibre collection efficiency at each channel, as will be later confirmed by back-focal plane imaging. The inset in Fig. 3d shows confocal PL scans of the SPE as imaged through the metalens in both LPx and LPy channels, normalised to the LPx maximum. The distinct emission from SPE as well as their signal-to-noise ratio are clearly visualised for each polarisation channel. The missing PSB peak is caused by the wavelength selectivity of the metalens, more discussion can be found in Supplementary Note 1.

To clarify that the detected photons are from the same SPE, 2<sup>nd</sup> order cross-correlation measurements between these PL channels are performed. Fig. 3e-f show cross-correlation measurements between the emitter PL in reflection (employing traditional objective) versus LPx and LPy (employing the metalens as the collecting lens), while Fig. 3g shows cross correlation between the two polarised channels LPx and LPy (using the metalens to collect the light). The same SPE with its corresponding quantum behaviour is verified across all three measurements, as all the  $g^{(2)}(0)$  values approximately equal to 0.1 (Fig. S4). The measurements also confirm the effectiveness of the metalens and its versatile use for low-intensity light collection - as demonstrated with quantum emitters in hBN. Furthermore, the lens efficiency and the independent sample substrate enables its use as an imaging lens. To this extent, the results of other SPEs are shown in the supporting information (Fig. S5).

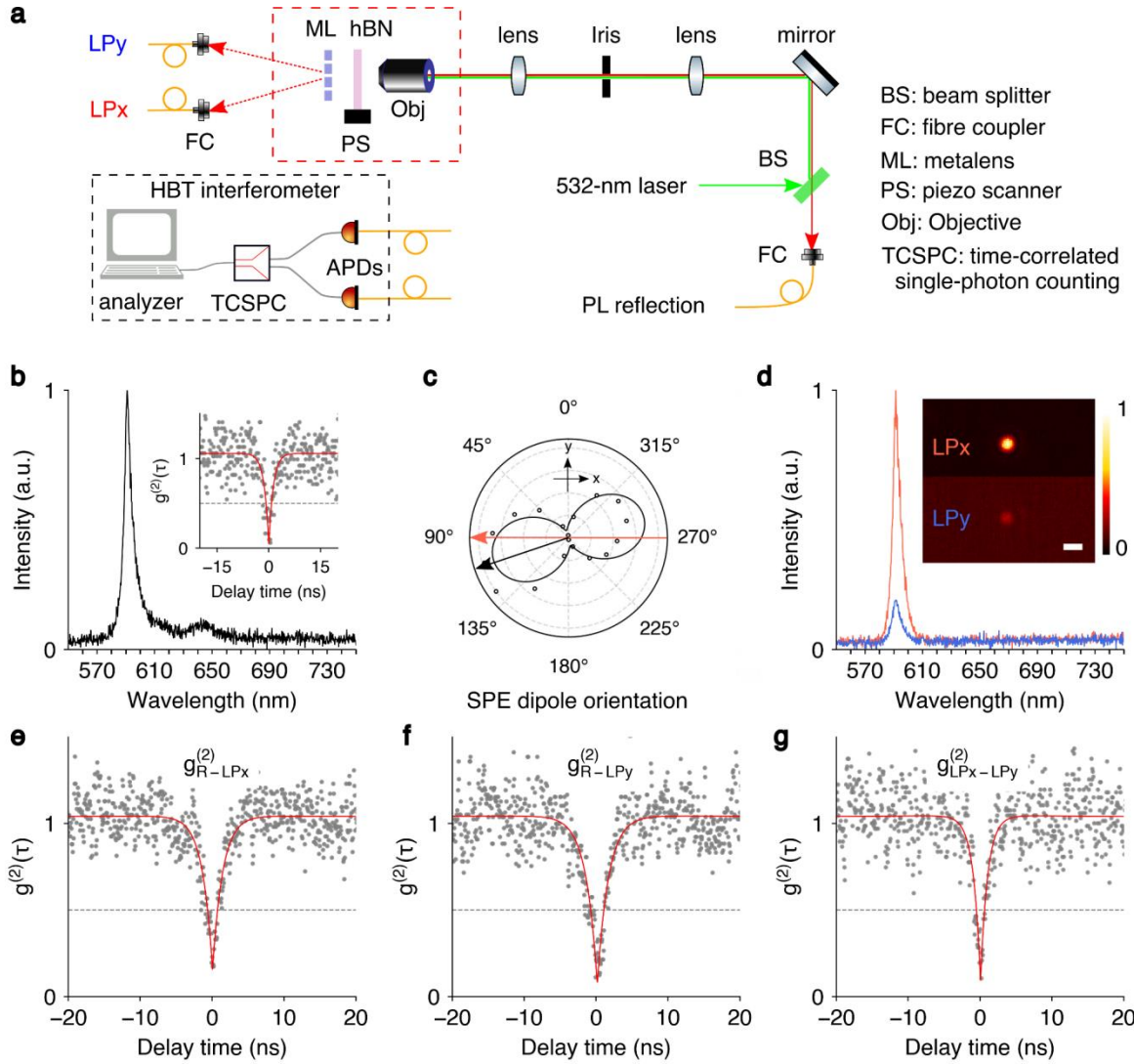


**Fig. 3: Characterisation of hBN SPEs with the polarisation beam-splitting metalens.** *a*, A schematic optical setup for the photonic measurement. *b*, PL collected via reflection channel (traditional objective) with a ZPL at  $\sim 591$  nm. Inset,  $g^{(2)}(\tau)$  confirmed the quantum nature of the SPE. *c*, emitter dipole orientation, measured from the reflection channel where  $0^\circ$  is the  $y$  (vertical) direction. The metalens orientation is set to  $90^\circ$  (red arrow). The emitter dipole orientation (black arrow) of  $106^\circ$  is derived after fitting with a sine function. *d*, PL spectra collected from LPx (red curve) and LPy (blue curve) polarised channels employing the metalens. Insets are corresponding PL raster maps of the emitter. Colour bars in two maps are set to the same for a clear intensity contrast. Scale bars are  $1 \mu\text{m}$ . *e-g* are cross correlation antibunching measurements from different channels. *e*, reflection PL and LPx correlation. *f*, reflection PL and LPy correlation. *g*, LPx and LPy correlation.  $g^{(2)}(\tau)$  data is background corrected.

After confirming the beam-splitting metalens efficiently collects and spatially separates polarisation streams of the emitted light from SPEs, we imprint different functionalities on the metalenses for multi-dimensional structuring of quantum emission. We design and fabricate four different metalenses with distinct functionalities and increasing complexity, as shown schematically in Fig. 4a. By employing the 8-step (16 step) phase meta-atoms, metalenses 1 (2) deflect LPx and LPy to angles of  $\pm 12.58^\circ$  ( $\pm 6.29^\circ$ ) along the x-direction, respectively. Metalens 3 deflects LPx and LPy in arbitrary directions, shifted from the centre, and finally, the 4th metalens encodes different helical phase fronts carrying distinctive OAM values ( $l=3$  and  $l=-1$ , in our case) - in addition to the directionality and polarisation. Fig. 4b shows the

far-field optical images of the fabricated four metalenses and their characteristic interference patterns. We then employ these metalenses to image the same SPE, as presented in Fig. 3.

The results of the four metalenses are shown in Fig. 4c. For convenience and clarity, we rotate the emitter to  $146^\circ$ , resulting in a dipole-to-metalens intersection angle of  $56^\circ$ , to balance the emission rate of the two channels (Fig. S6). The white dash circles in the images represent the maximum splitting angle of  $25^\circ$ , while the inset red (blue) circle is a zoomed-in image of the LP<sub>x</sub> (LP<sub>y</sub>) spot. In the first metalens we observed two bright spots, and the PL signals (summed in Ky direction) gave a clear peak profile of the two spots with an intensity ratio of  $A_{LPy}/A_{LPx} = 1.28$ , aligned well with the predicted ratio of  $\tan(56^\circ) = 1.48$ . The second metalens demonstrates axial symmetric deflection with a half splitting angle compared to the former one. As expected, the emitters are imaged closer, with a smaller deflection angle and spot intensity ratio of  $A_{LPy}/A_{LPx} = 1.40$ . The third metalens splits the incoming SPE asymmetrically, with two spots falling into the same side and also deflected in the y axis ( $A_{LPy}/A_{LPx} = 5.08$ ). The combination of the three presented metalenses hence allows for complete direction and polarisation control of the imaged SPEs. As a final demonstration, the fourth metalens shows two doughnut beams (zoomed-in in the insets) that correspond to the OAM with topological charges of  $l=3$  and  $l=1$  for the LP<sub>x</sub> and LP<sub>y</sub> channels, respectively. Since the larger OAM leads to larger doughnut intensity distribution in the momentum space, LP<sub>y</sub> becomes brighter than LP<sub>x</sub> ( $A_{LPy}/A_{LPx} = 2.29$ ). As a result, our metalens conclusively demonstrates a complete control of single photons in directionality, polarisation and OAM dimensions, simultaneously.

To support these results, we have also performed scalar wave propagation calculations. Complex-amplitude profiles were extracted from the four metalenses with two polarisation channels, then modified by assuming the dipole source is located at the exact focal position (subtraction of lens phase in each profile). First, each modified profile with the two polarisation channels was used to evaluate far-field profiles using Rayleigh-Sommerfeld (RSD) diffraction integral. Then, far-field images in the LP<sub>x</sub> and LP<sub>y</sub> channel were directly integrated by considering the polarisation angle of the dipole source (Fig. 4c bottom panel). Each metalens performs the desired function well, showing a clear collimated beam that is successfully structured as designed.

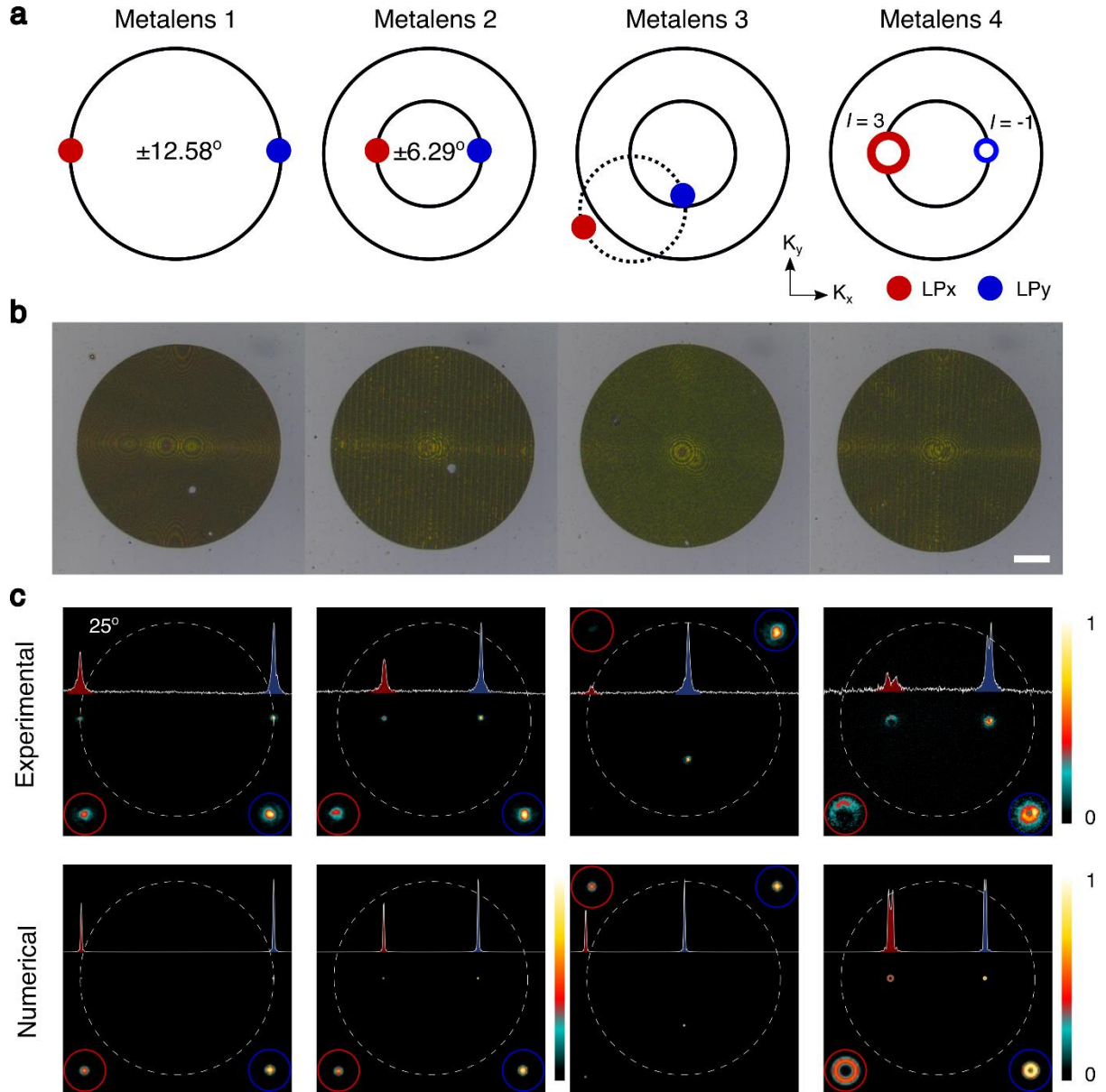


**Fig. 4: Arbitrary structured quantum emission with polarising beam-splitting metalenses.** *a*, Schematics of different metalens functionalities. The circles represent desired positions for orthogonal linear polarisations in the  $k$  space. The doughnut-shaped spots indicate the generation of OAM. *b*, far-field optical images of the fabricated metalenses. Scale bar is  $30 \mu\text{m}$ . *c*, experimental (top) and numerically calculated (bottom) results of the SPE far-field back focal imaging. Curves in *c* represent the vertically accumulated PL intensity of the LPx (filled with red) and LPy (filled with blue). The red and blue circles are zoomed-in insets for highlighting the intensity distributions of the orthogonal polarisations.

## Conclusion

In this work, we proposed and implemented a multifunctional metalens to arbitrarily structure quantum light sources at room temperature. Realised with bright and linearly polarised SPEs in hBN, our designed and fabricated polarisation beam-splitting metalens allows independent wavefront shaping of orthogonal linear polarisations. We further experimentally demonstrated arbitrary directionality control



of single photon emission, as well as imprinting different OAM modes onto its orthogonal polarisations. As such, our demonstration offers a new platform to use ultrathin meta-optics for arbitrary wavefront shaping of quantum emission in multiple degrees of freedom at room temperature. It may provide new insights into the field of quantum information science - specifically manipulating photon polarisations has great impact for quantum cryptography and entanglement distribution with improved filtering. The polarisation separation is vital, for future employment of hBN SPEs for polarisation entangled photon pair generation, as it is commonly used for down converted photon sources<sup>29</sup>.

Moreover, our imaging metalens endows a direct access to the OAM states of single photons, offering a compact platform for high-dimensional quantum entanglement to increase the quantum information capacity<sup>30, 31, 32</sup>. Future extension of the metalens to realise higher-order structured vector beams<sup>33</sup> could enable the generation of high-dimensional single-photon hybrid quantum states.. Furthermore, future integration of structured SPE source with a reliable transmission environment such as optical fibre<sup>34</sup> could promise a quantum network with higher information capacity, robustness to noise and better security. Lastly, we envision that combining the spin defects in hBN with the proposed multifunctional metalens may enable efficient spin photon readout and remote quantum sensing<sup>35, 36, 37, 38, 39</sup>.

## Methods

### Acknowledgments

The authors thank Milos Toth, Yongliang Chen and Simon White for their fruitful discussion. This work was supported by Australian Research Council (CE200100010, DE220101085, DP220102152) and the Office of Naval Research Global (N62909-22-1-2028)(I.A.).

S.A.M. acknowledges the Lee-Lucas Chair in Physics.

J.R. acknowledges funding supports from POSCO-POSTECH-RIST Convergence Research Center program funded by POSCO and the National Research Foundation (NRF) grants (NRF-2022M3C1A3081312, NRF-2022M3H4A1A02085335, NRF-2022M3H4A1A02074314, NRF-2019R1A2C3003129, CAMM2019M3A6B3030637, NRF-2019R1A5A8080290) funded by the Ministry of Science and ICT (MSIT) of the Korean government. J.H.K. acknowledges the POSTECH Alchemist fellowship.

### Author Contributions

I.A., H.R., and J.R. conceived the concept of this project. C.L. prepared SPEs and conducted the SPE-metalens measurements. J. J. conducted optical characterisation of the metalenses. T.B. and J.J. designed the metalenses. J.H.K. and J.K.K. fabricated the metalenses. C.L., T.Y. and M.N. built the photonic characterisation platform for the SPE-metalens system. C.L., J.J., T.B. and H.R. analysed the data. All authors discussed the results and wrote the manuscript.

### Competing interests

The authors declare that they have no competing interests.

### References

1. Awschalom DD, Hanson R, Wrachtrup J, Zhou BB. Quantum technologies with optically interfaced solid-state spins. *Nature Photonics* 2018, **12**(9): 516-527.
2. Liu X, Hersam MC. 2D materials for quantum information science. *Nature Reviews Materials* 2019, **4**(10): 669-684.
3. Tran TT, Bray K, Ford MJ, Toth M, Aharonovich I. Quantum emission from hexagonal boron nitride monolayers. *Nat Nanotechnol* 2016, **11**(1): 37-41.
4. Caldwell JD, Aharonovich I, Cassabois G, Edgar JH, Gil B, Basov DN. Photonics with hexagonal boron nitride. *Nature Reviews Materials* 2019, **4**(8): 552-567.
5. Hayee F, Yu L, Zhang JL, Ciccarino CJ, Nguyen M, Marshall AF, *et al.* Revealing multiple classes of stable quantum emitters in hexagonal boron nitride with correlated optical and electron microscopy. *Nat Mater* 2020, **19**(5): 534-539.
6. Senellart P, Solomon G, White A. High-performance semiconductor quantum-dot single-photon sources. *Nat Nanotechnol* 2017, **12**(11): 1026-1039.
7. Dorrah AH, Capasso F. Tunable structured light with flat optics. *Science* 2022, **376**(6591): eabi6860.
8. Tseng ML, Semmlinger M, Zhang M, Arndt C, Huang TT, Yang J, *et al.* Vacuum ultraviolet nonlinear metalens. *Sci Adv* 2022, **8**(16): eabn5644.

9. Santiago-Cruz T, Gennaro SD, Mitrofanov O, Addamane S, Reno J, Brener I, *et al.* Resonant metasurfaces for generating complex quantum states. *Science* 2022, **377**(6609): 991-995.
10. Solntsev AS, Agarwal GS, Kivshar YS. Metasurfaces for quantum photonics. *Nature Photonics* 2021, **15**(5): 327-336.
11. Ni J, Huang C, Zhou LM, Gu M, Song Q, Kivshar Y, *et al.* Multidimensional phase singularities in nanophotonics. *Science* 2021, **374**(6566): eabj0039.
12. Li L, Liu Z, Ren X, Wang S, Su VC, Chen MK, *et al.* Metalens-array-based high-dimensional and multiphoton quantum source. *Science* 2020, **368**(6498): 1487-1490.
13. Wang K, Titchener JG, Kruk SS, Xu L, Chung HP, Parry M, *et al.* Quantum metasurface for multiphoton interference and state reconstruction. *Science* 2018, **361**(6407): 1104-1108.
14. Ren H, Jang J, Li C, Aigner A, Plidschun M, Kim J, *et al.* An achromatic metafiber for focusing and imaging across the entire telecommunication range. *Nat Commun* 2022, **13**(1): 4183.
15. Badloe T, Kim I, Kim Y, Kim J, Rho J. Electrically Tunable Bifocal Metalens with Diffraction-Limited Focusing and Imaging at Visible Wavelengths. *Adv Sci* 2021, **8**(21): e2102646.
16. Joo WJ, Kyoung J, Esfandyarpour M, Lee SH, Koo H, Song S, *et al.* Metasurface-driven OLED displays beyond 10,000 pixels per inch. *Science* 2020, **370**(6515): 459-463.
17. Ni X, Kildishev AV, Shalaev VM. Metasurface holograms for visible light. *Nature Communications* 2013, **4**(1): 1-6.
18. Ren H, Fang X, Jang J, Burger J, Rho J, Maier SA. Complex-amplitude metasurface-based orbital angular momentum holography in momentum space. *Nat Nanotechnol* 2020, **15**(11): 948-955.
19. So S, Kim J, Badloe T, Lee C, Yang Y, Kang H, *et al.* Multicolor and 3D holography realized by inverse design of single-celled metasurfaces. *arXiv preprint arXiv:04778* 2022.
20. Li SQ, Xu X, Maruthiyodan Veetil R, Valuckas V, Paniagua-Dominguez R, Kuznetsov AI. Phase-only transmissive spatial light modulator based on tunable dielectric metasurface. *Science* 2019, **364**(6445): 1087-1090.
21. Kim I, Kim WS, Kim K, Ansari MA, Mehmood MQ, Badloe T, *et al.* Holographic metasurface gas sensors for instantaneous visual alarms. *Sci Adv* 2021, **7**(15): eabe9943.
22. Yang F, Jha PK, Akbari H, Bauser HC, Atwater HA. A hybrid coupler for directing quantum light emission with high radiative Purcell enhancement to a dielectric metasurface lens. *Journal of Applied Physics* 2021, **130**(16): 163103.
23. Huang TY, Grote RR, Mann SA, Hopper DA, Exarhos AL, Lopez GG, *et al.* A monolithic immersion metalens for imaging solid-state quantum emitters. *Nat Commun* 2019, **10**(1): 2392.
24. Bao Y, Lin Q, Su R, Zhou ZK, Song J, Li J, *et al.* On-demand spin-state manipulation of single-photon emission from quantum dot integrated with metasurface. *Sci Adv* 2020, **6**(31): eaba8761.
25. Wu C, Kumar S, Kan Y, Komisar D, Wang Z, Bozhevolnyi SI, *et al.* Room-temperature on-chip orbital angular momentum single-photon sources. *Sci Adv* 2022, **8**(2): eabk3075.

26. Knall EN, Knaut CM, Bekenstein R, Assumpcao DR, Stroganov PL, Gong W, *et al.* Efficient Source of Shaped Single Photons Based on an Integrated Diamond Nanophotonic System. *arXiv preprint arXiv:220102731* 2022.
27. Yang Y, Yoon G, Park S, Namgung SD, Badloe T, Nam KT, *et al.* Revealing Structural Disorder in Hydrogenated Amorphous Silicon for a Low-Loss Photonic Platform at Visible Frequencies. *Adv Mater* 2021, **33**(9): e2005893.
28. Yoon G, Kim K, Huh D, Lee H, Rho J. Single-step manufacturing of hierarchical dielectric metalens in the visible. *Nat Commun* 2020, **11**(1): 2268.
29. Kwiat PG, Mattle K, Weinfurter H, Zeilinger A, Sergienko AV, Shih Y. New high-intensity source of polarization-entangled photon pairs. *Phys Rev Lett* 1995, **75**(24): 4337-4341.
30. Mair A, Vaziri A, Weihs G, Zeilinger A. Entanglement of the orbital angular momentum states of photons. *Nature* 2001, **412**(6844): 313-316.
31. Fickler R, Lapkiewicz R, Plick WN, Krenn M, Schaeff C, Ramelow S, *et al.* Quantum entanglement of high angular momenta. *Science* 2012, **338**(6107): 640-643.
32. Malik M, Erhard M, Huber M, Krenn M, Fickler R, Zeilinger A. Multi-photon entanglement in high dimensions. *Nature Photonics* 2016, **10**(4): 248-252.
33. Forbes A, de Oliveira M, Dennis MR. Structured light. *Nature Photonics* 2021, **15**(4): 253-262.
34. Cozzolino D, Bacco D, Da Lio B, Ingerslev K, Ding Y, Dalgaard K, *et al.* Orbital Angular Momentum States Enabling Fiber-based High-dimensional Quantum Communication. *Physical Review Applied* 2019, **11**(6): 064058.
35. Gottscholl A, Diez M, Soltamov V, Kasper C, Krausse D, Sperlich A, *et al.* Spin defects in hBN as promising temperature, pressure and magnetic field quantum sensors. *Nat Commun* 2021, **12**(1): 4480.
36. Stern HL, Gu Q, Jarman J, Eizagirre Barker S, Mendelson N, Chugh D, *et al.* Room-temperature optically detected magnetic resonance of single defects in hexagonal boron nitride. *Nat Commun* 2022, **13**(1): 618.
37. Chejanovsky N, Mukherjee A, Geng J, Chen YC, Kim Y, Denisenko A, *et al.* Single-spin resonance in a van der Waals embedded paramagnetic defect. *Nat Mater* 2021, **20**(8): 1079-1084.
38. Gao X, Vaidya S, Li K, Ju P, Jiang B, Xu Z, *et al.* Nuclear spin polarization and control in hexagonal boron nitride. *Nat Mater* 2022, **21**(9): 1024-1028.
39. Robertson IO, Tan C, Scholten SC, Healey AJ, Abrahams GJ, Zheng G, *et al.* Imaging current control of magnetization in Fe<sub>3</sub>GeTe<sub>2</sub> with a widefield nitrogen-vacancy microscope. *arXiv preprint arXiv:220710329* 2022.